Mon. Not. R. Astron. Soc. **399,** 432–442 (2009) doi:10.1111/j.1365-2966.2009.15295.x

# Are pre-main-sequence stars older than we thought?

Tim Naylor★

*School of Physics, University of Exeter, Stocker Road, Exeter EX4 4QL*

Accepted 2009 June 23. Received 2009 June 16; in original form 2009 March 23

**ABSTRACT**

We fit the colour–magnitude diagrams of stars between the zero-age main-sequence and terminal-age main sequence in young clusters and associations. The ages we derive are a factor of 1.5–2 longer than the commonly used ages for these regions, which are derived from the positions of pre-main-sequence stars in colour–magnitude diagrams. From an examination of the uncertainties in the main-sequence and pre-main-sequence models, we conclude that the longer age scale is probably the correct one, which implies that we must revise upwards the commonly used ages for young clusters and associations. Such a revision would explain the discrepancy between the observational lifetimes of protoplanetary discs and theoretical calculations of the time to form planets. It would also explain the absence of clusters with ages between 5 and 30 Myr.

We use the $\tau^2$ statistic to fit the main-sequence data, but find that we must make significant modifications if we are to fit sequences which have vertical segments in the colour–magnitude diagram. We present this modification along with improvements to the methods of calculating the goodness-of-fit statistic and parameter uncertainties.

Software implementing the methods described in this paper is available from http://www.astro.ex.ac.uk/people/timn/tau-squared/.

**Key words:** methods: statistical – stars: early-type – stars: formation – stars: fundamental parameters – stars: pre-main-sequence – open clusters and associations: general.

## 1 INTRODUCTION

The ability to determine the ages of pre-main-sequence (PMS) stars is crucial for advancing our understanding of the early phases of stellar evolution. There are two key applications. First, and perhaps most obviously, we need stellar ages if we are to carry out experiments, such as tracing the evolution of stellar angular momentum or following the fraction of stars with protoplanetary discs as a function of time. Secondly, for PMS stars, the conversion from observables such as temperature and luminosity into mass is highly age-dependent, making accurate ages vital for determining the mass function. The primary method of determining the ages required for these studies is to compare the observed properties of PMS stars with models. The most easily accessible observables are a star's temperature and luminosity, since they can be measured from its colours and magnitudes. The problem is that for the same colours and magnitudes different models can predict ages which differ by a factor of 2, and even the same models will predict different ages depending on which colours and magnitudes are used. This makes meaningful comparisons between the ages quoted in the literature for clusters or associations at best difficult, and often impossible. It was these problems which led us to devise a model-independent age ordering of young clusters and associations based on their colour–magnitude diagrams (Mayne et al. 2007). For PMS stars, the primary age diagnostic is based on the fact that stars fade as they get older and contract towards the main sequence (MS). We used this movement of the sequence towards progressively fainter magnitudes to derive an age ordering, although to do so we also had to measure a consistent set of distances, which we derived from the more massive stars which have already reached the MS (Mayne & Naylor 2008).

Whilst an age ordering such as ours is useful, for example it has showed unambiguously that different clusters take different times to reach the same disc fraction or angular momentum distribution, for quantitative work an absolute scale is required. For PMS clusters and associations, there are several usable age indicators, each of which relies on comparing stellar properties with models. For this reason, it is best to group them according to the underlying physics. First is the contraction of PMS stars as they approach the MS. As pointed out above, and discussed at length in Mayne et al. (2007), these 'contraction' or 'PMS' ages are highly model-dependent, and given the current disagreements between the models cannot yield an absolute age scale. Although most stars in a young cluster or association are in the PMS phase, the evolution of the most massive stars proceeds so fast that they may not only have reached the MS, but evolved beyond it. This gives us access to two more age measures.

★E-mail: timn@astro.ex.ac.uk

First, having reached the MS, stars move redwards and to higher luminosities away from the zero-age main-sequence (ZAMS), due to the increasing helium content of their cores. This movement continues until the point of core hydrogen exhaustion, when the star has reached the reached the terminal age MS (MS turn-off). Finally, after the turn-off, the post-MS evolution is driven by the burning of heavier elements which leads to much more rapid movement in the CMD. This relatively high velocity in the CMD means that post-MS evolution has the potential to give precise ages. However, for young Galactic clusters the paucity of stars in this region of the CMD means such an age can depend on just one star, and such ages are rightly treated with some scepticism. Conversely, the MS evolution (from the ZAMS to the turn-off) has a larger number of stars, but the movement is often subtle, and using the normal technique of simply plotting isochrones over the data leads to large uncertainties in age, and to questions over objectivity. However, we have been developing a method of making objective fits to colour–magnitude data, which should allow us to unlock the information in this stage of a star's evolution. The technique, called $\tau^2$ fitting, can be viewed as an extension of $\chi^2$ to data points with uncertainties in two or more observables, and to models which are distributions (not just lines) in the data space.

The aim of this paper is to apply the $\tau^2$-fitting technique to the MS evolution of young stars, and use the resulting ages to create a revised age scale for PMS stars. Surprisingly, this leads to significantly older ages than the commonly used contraction ages, a result which we will discuss in Section 11. To derive this result, we first have to update our statistical techniques originally described in Naylor & Jeffries (2006), since, as we discuss in Section 4, the technique will not work for the isochrones we wish to fit. We therefore lay out the changes which need to be made by following an example through fitting (Section 5), testing the goodness of fit (Section 6) and determining the uncertainties in the derived parameters (Section 7). Before doing so, however, we discuss the data and models we use (Sections 2 and 3). We deal with the effects of interstellar extinction in Section 8, and the details of each cluster in Section 9. We draw all the results together in our discussion in Section 11.

## 2 THE DATA

To compare a set of ages derived from MS evolution with contraction ages, we need a sample of clusters and associations which have contraction ages, and for each of which data are available for MS fitting. Our sample is, therefore, based on the groups we placed in age order using the PMS in Mayne & Naylor (2008). Clearly, for each of these groups we require stars in the appropriate mass range to show significant MS evolution, but we also require extinctions and reliable distance measurements. *UBV* photometry can provide all three of these. First, the $U - B/B - V$ diagram provides extinctions. Secondly, the upper part of $V/B - V$ diagram is age-sensitive, tracing the evolution of stars from the ZAMS to the turn-off. Finally, in the age range of interest the lower mass stars are still close to the ZAMS, and the sequence turns redwards, making it ideal as a distance measure. Furthermore, the *UBV* photoelectric system is very consistent and well characterized. However, to ensure we maintain the highest level of consistency we have restricted ourselves as far as possible to the data of Johnson and collaborators, primarily taken in the 1950s and 1960s. As we shall show later, the quality of these data when combined with the transformations of Bessell, Castelli & Plez (1998) is impressive, giving $\tau^2$ values which means that the model is a good fit to the data. Clearly, we wish to avoid PMS stars contaminating our sample at faint magnitudes and red colours, and so for most objects we apply a cut in observed $B - V$ which roughly corresponds to $(B - V)_0 < 0.0$.

Most of the data sets we use have robust uncertainties derived from comparisons of many measurements of stars. This presents us with a problem, as the quoted uncertainties in colour are always smaller than those in magnitude. Conventional error analysis yields a correlation between, say, $V$ and $B - V$, and in previous work we have always been careful to include that correlation when modelling the uncertainties. The starting point for such an analysis is that $V$ and $B$ are measured independently, and so the uncertainties in $V$ and $B - V$ are $\delta V$ and $\sqrt{\delta V^2 + \delta B^2}$, respectively. Such an analysis also leads to the conclusion that the uncertainty in $B - V$ must be larger than that in $V$, in direct contradiction to the quoted uncertainties for most of the data presented here. This is because it is not photon statistics which are the driver of the uncertainties, but changes in the transparency. In this work, we therefore model the uncertainties as uncorrelated.

## 3 THE MODELS

Although we will try other models later, we begin by using 'Geneva–Bessell' isochrones. For the stellar interior, we follow the suggestion of Lejeune & Schaerer (2001), and use the 'basic model set' (i.e. set 'c') of the Geneva isochrones (Schaller et al. 1992). Temporal interpolation is a much more significant issue for post-MS isochrones than the PMS isochrones we have fitted in the past, as there are sharp discontinuities in the rate of change of magnitude and colour with time, as exemplified by the MS turn-off. We therefore use the code provided on the web site to interpolate the isochrones to the appropriate age. We then convert from luminosity and effective temperature to colours and magnitudes using the tables of Bessell et al. (1998), assuming that the colours of Vega are zero (though $V = 0.03$). We also use Bessell et al.'s colour-dependent extinction vectors.

For some of the most luminous stars, the gravities are rather low, and fall just outside the range of gravities given by Bessell et al. (1998). In these cases, we extrapolate the models by simply setting the colour to that for the lowest available gravity. In these cases, a linear extrapolation would be different by less than 0.001 mag, implying that the overall error due to the extrapolation is much smaller than the uncertainties in colour.

For reasons explained in Section 9.2, we used the Tycho-2 photometry for $\sigma$ Ori. In this case, we have used the conversion given in Bessell (2000) to convert the Geneva–Bessell isochrones into the Tycho system. (Høg et al. 2000a, state that the Tycho-1 and Tycho-2 systems should be identical.) We used the reddening vector derived in Mayne & Naylor (2008).

## 4 STATISTICS

In Naylor & Jeffries (2006), we introduced a solution to the long-standing problem of how to fit photometric data to isochronal models in colour–magnitude diagrams (CMDs). Whilst fitting an isochronal model (a curve) to a set of data points may at first appear to be a simple $\chi^2$ problem, the facts that the data points have uncertainties in two dimensions and that the curve is smeared by binarity into a two-dimensional distribution mean a more sophisticated technique is required. We have now used our solution to derive ages and distances for the young clusters NGC 2547 (Naylor & Jeffries 2006) and NGC 2169 (Jeffries et al. 2007), and consistent distances to some of the best-studied star-forming regions (Mayne & Naylor 2008). In Jeffries et al. (2009), we derive distances to Vel

OB2 and the association around $\gamma$ Vel, and Joshi et al. (2008) use our technique for measuring the distance to NGC 7419.

Naylor & Jeffries (2006) provide a rigorous development of $\tau^2$, but for the purpose of understanding the improvements we have had to make to the method, a relatively simple intuitive interpretation gives a better insight into the problems. Fig. 1 shows a typical fit of a data set (shown as circled error bars) to a model (the colour scale). The model is a simulation of roughly a million stars (including binaries) using a specific age, metallicity, mass function and distance, which is then sampled on to a grid in colour–magnitude space. A fit in (e.g.) distance can be viewed as moving the model in the $y$-direction until one obtains the strongest overlap between the model and the data. This overlap can be quantified for a single data point by taking the function which represents its position and uncertainties (normally a two-dimensional Gaussian), multiplying it on a gridpoint-by-gridpoint basis by the grid, and then summing the resulting values. If the grid is $\rho(c, m)$ (where $c$ and $m$ are the colour and magnitude coordinates, respectively) and the $i$th data point and its uncertainties $U_i(c - c_i, m - m_i)$ (where $c_i$, $m_i$ are its coordinates), then mathematically the overlap is the integral of $U_i\rho$ over the entire space. The product of these integrals for all the data points will therefore reflect the overall overlap between the data points and the model, and so we define a statistic

$$\tau^2 = -2 \sum_{i=1,N} \ln \int U_i(c - c_i, m - m_i)\rho(c, m)\mathrm{d}c\ \mathrm{d}m, \qquad (1)$$

whose minimum value corresponds to the best fit.

In Naylor & Jeffries (2006), we showed that this definition will, for models which are curves in $(c, m)$ space, and only have uncertainties in the $m$-axis, reduce to that for $\chi^2$. However, this is only the case if one chooses to multiply $\rho$ by a normalization factor which is dependent on the gradient of the isochrone. Unfortunately, this normalization factor becomes infinite if the isochrone is vertical, and double-valued at any magnitude at which the isochrone is double-valued. This means our $\chi^2$-like normalization will fail for the CMD fitting required here, because as one moves up the sequence towards bright magnitudes the isochrones become vertical, before finally switching to a negative gradient. Furthermore, if we wish to fit in $U - B/B - V$ space, the isochrones are double-valued for certain values of $B - V$.

In what follows, we therefore develop an alternative normalization, which allows us to fit the data. In doing so, we expose the limitations of an approximation we made when calculating the probability that the data are a good fit to the model.

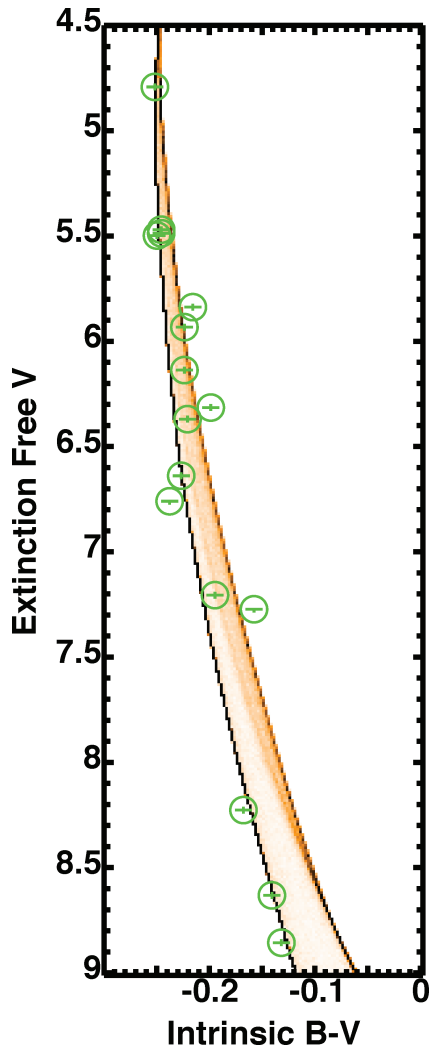


**Figure 1.** The data and best-fitting model for Cep OB3b. The colour scale is the model ($\rho$ in equation 1) and the encircled error bars are the data.

## 5 FITTING THE DATA

### 5.1 The model CMD

We must first create a probability density function to fit to the data. As in Naylor & Jeffries (2006), we create this by simulating stars over the appropriate range of masses. For each star, we choose a mass randomly from the Salpeter IMF, and if the star is a binary we assign it a companion of a mass drawn from a uniform distribution between zero and the mass of the primary. The stellar model then provides a luminosity, gravity and effective temperature for each star, which we then convert into colour and magnitude using the appropriate bolometric corrections. If a binary companion is so low mass, or so cool, that it does not appear in the models, it is assigned a flux of zero. [Note that this assignment is a change from Naylor & Jeffries (2006), but has been used in all our subsequent work.] The value of each pixel in the image is then simply the number of stars whose colours and magnitudes lie within the pixel. We typically simulate $10^6$ stars, and for this work we have used pixels of size 0.0025 mag in each axis. This is half the value we have used in the previous work, but is necessitated by the small uncertainties of the current data. We find that the residual effects of the placement of pixel boundaries are much smaller ($\sim$0.005 mag in derived distance modulus) than the uncertainties in derived parameters.

### 5.2 The normalization of $\rho$

Before proceeding further, we must address the normalization of the model image, $\rho$. In Naylor & Jeffries (2006), we used our $\chi^2$-like normalization which was a function of magnitude. Here, we instead explore the results of a much simpler normalization, setting the integral of $\rho$ over the entire image to one. This raises the question of how faint a magnitude we must integrate down to. In fact, the strictly correct way to proceed would be to first multiply the image by the photometric completeness function, such that below a certain magnitude $\rho$ was zero, and then set the integral of what remains to one. Such a normalization has an interesting, though subtle implication. When fitting for distance modulus as the distance modulus increases, there is a decrease in the non-zero area

of $\rho$, the region between the faintest observable absolute magnitude (as defined by the completeness function) and the brightest model star. Given that the integral over the model remains one, this means the value of any non-zero pixel will increase, implying that $\tau^2$ will decrease, and hence the fit will improve. This is actually the correct behaviour, since it means that a model which fully populates the upper part of the sequence is better than one which does not. Practically, for our data, we can use a simpler normalization, where we make the integral between the faintest and the brightest data points one. This means that we have thrown away one possible source of information, but in practice this does not significantly affect the fits.

Comparing the results obtained using this normalization with that used in Naylor & Jeffries (2006) simply changes the values of $\tau^2$ in a given $\tau^2$ parameter grid by an additive factor; it does not change the best-fitting parameters. This is at first a surprising result since we are changing the value of $\rho$ in one part of the isochrone compared with another, which may appear as a weighting of the points. However, it should be remembered that adding the logarithms of the integrals in equation (1) is equivalent to multiplying them together, so changing the relative values of $\rho$ as a function of magnitude is a normalization, not a weighting process. The only possibility for altering the best fit is if the length-scale for changes in $\rho$ is small compared to the size of an error bar. Then, data points will drag the fit so that they lie in the higher valued regions of $\rho$. Since the data point is more likely to originate in the higher density part of the model, this would again be the correct behaviour.

Finally, it is important to note that we have no longer 'normalized out' the mass function as we did in Naylor & Jeffries (2006). Changing the mass function will change the value of $\tau^2$. In practice, we have chosen to fix it such that $\mathrm{d}N/\mathrm{d}M \propto -2.35$, which results in good fits to the models.

### 5.3 The normalization of *U*

If we are to change the normalization of the model, we must also consider the normalization of the uncertainty function ($U$ in equation 1). In $\chi^2$ fitting, this is set such that the maximum value of $U$ is always the same, so the highest probability attainable is always the same, corresponding to a perfect fit, i.e. $\chi^2 = 0$. This is the normalization we adopted in Naylor & Jeffries (2006). However, there is another obvious possibility, setting the integral of $U$ to be one. This would have a very significant advantage in cases where the error bars seem to have been significantly underestimated, and to obtain a good fit [i.e. a value of $\tau^2$ which corresponds to a $\Pr(\tau^2)$ of approximately 0.5] one has to add an extra uncertainty to $U$, in addition to those from the observations. This could well be due to mismatches between photometric systems. In such cases, the procedure we have previously adopted has been to calculate $\tau^2$, and then $\Pr(\tau^2)$ for increasing values of the added uncertainty, until $\Pr(\tau^2)$ exceeds 0.5. However, if one normalizes $U$ such that its integral is one, then conceptually one is comparing a model which includes the uncertainties with data points which are $\delta$-function. One can, therefore, simply adjust the values of the uncertainties until one obtains the lowest value of $\tau^2$.

This normalization has an additional conceptual advantage. In the case where the uncertainties are very small one can now approximate $U$ as two-dimensional $\delta$-functions. This effectively removes the integral in equation (1), and means that one can evaluate $\tau^2$ by simply multiplying together the values of $\rho$ at the positions of the data points.

We will refer to a normalization where the integral of the models and the integrals of the uncertainty functions are all one as the natural normalization. This clearly distinguishes it from the $\chi^2$-like normalization used in Naylor & Jeffries (2006).

### 5.4 The fit

Given that we now have the correct normalizations, we can now fit our example data, which is a sample from Cep OB3b described in detail in Section 9.6. We calculated the extinction on a star-by-star basis as described in Section 8, and corrected for it. We then evaluated equation (1) at values of the age and distance modulus which cover the range of interest. The resulting $\tau^2$ space is shown in Fig. 2. The best fit, which lies at 10 Myr and a true distance modulus of 8.7 mag, is shown overlaid on the data in Fig. 1.

In some fits, we find that there are data points which clearly do not lie on the sequence and are presumably non-members. To deal with these objects, we first fit the data with a variant of the 'soft clipping' first described in section 7.1 of Naylor & Jeffries (2006). We adapt this to the new normalization by imposing a maximum $\tau^2$ for any one data point. The value used is the minimum value of $\tau^2$ amongst all the data points, plus a fixed value, normally 20. We implement this by calculating the probability corresponding to the imposed maximum $\tau^2$ and adding this to the calculated probabilities for each data point before calculating their $\tau^2$ values. We then performed a second fit removing the data points which had $\tau^2$ values close to the clipping limit, with no clipping limit applied.

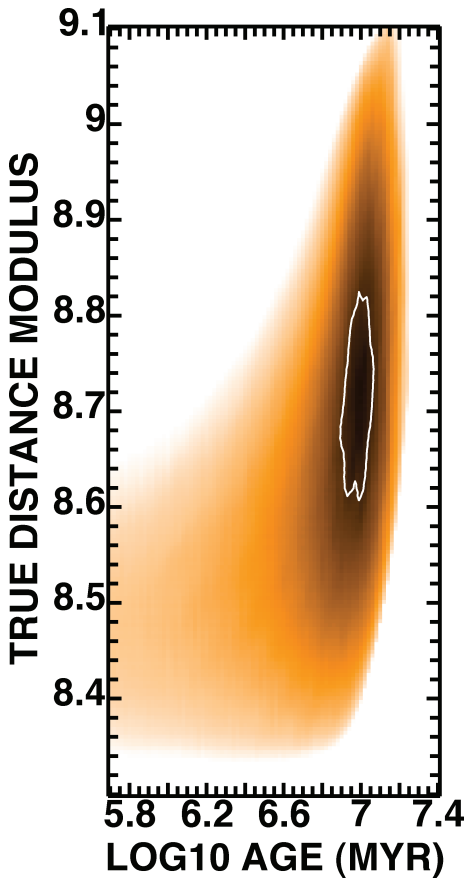


**Figure 2.** The $\tau^2$ grid for Cep OB3b. The contour is at the 68 per cent confidence level.

## 6 IS THE MODEL A GOOD FIT?

To test whether the model is a good fit, one must evaluate the chance of obtaining a given $\tau^2$ or below. One does this by calculating $\Pr(\tau^2)$, the cumulative distribution of the expected value of $\tau^2$. In Naylor & Jeffries (2006), we showed how to calculate this, for no free parameters, in such a way that it was insensitive to an incorrect choice of mass function. We then suggested that one allow for free parameters by multiplying the $\tau^2$-axis of the distribution by $(N - n)/N$.

Although our numerical simulations in Naylor & Jeffries (2006) showed that the above approach to the free parameter problem may be approximately correct for the $\chi^2$-like normalization, it is straightforward to show that it cannot be correct in an arbitrary normalization, such as the one described in Section 5.2. Consider a plot of the cumulative distribution of $\Pr(\tau^2)$ as a function of $\tau^2$ (Fig. 3). Changing the normalization of the model means multiplying $\rho$ in equation (1) by a constant. This has the effect of adding a constant to the values of $\tau^2$ as shown by the solid curves in Fig. 3. Allowing for free parameters by scaling the $\tau^2$-axis of the distribution by $(N - n)/N$ would yield different values for the decrease in $\tau^2$ when adding extra parameters, depending on the normalization. This cannot be correct, the decrease must be additive for the shape of the distribution to be invariant for a change in normalization.

There is an approximate solution to this problem, though, based on the fact that for CMD fitting the distribution of $\Pr(\tau^2)$ is similar to $\Pr(\chi^2)$, save an additive factor. The reason for this is that both distributions derive from the distribution of probability, and therefore $\tau^2$, in the CMD plane. For a $\chi^2$ problem, this distribution is a line, smeared by a one-dimensional Gaussian. For the $\tau^2$ CMD problem, the distribution approximates to two sequences (those of single stars and of equal-mass binaries) smeared by a two-dimensional Gaussian. It is, therefore, unsurprising that the resulting distributions of $\Pr(\tau^2)$ and $\Pr(\chi^2)$ are similar. So we could approximate $\Pr(\tau^2)$ by simply using the $\chi^2$ distribution directly. However, for large values of $N - n$ the differential form of the $\chi^2$ distribution tends to a normal distribution whose mean is $N - n$ and $\sigma$ is $2(N - n)$.[1] This means that we can allow for $n$ free parameters by subtracting the expectation value from the distribution of $\tau^2$, multiplying the $\tau^2$-axis by $(N - n)/N$, and adding back the expectation value less $n$. We have implemented the latter approach, as it retains any asymmetry in the distribution. Applying this to the Cep Ob3b data results in a value of $\Pr(\tau^2)$ of 0.05. This is on the margins of acceptability, but no single data point is clearly discrepant.

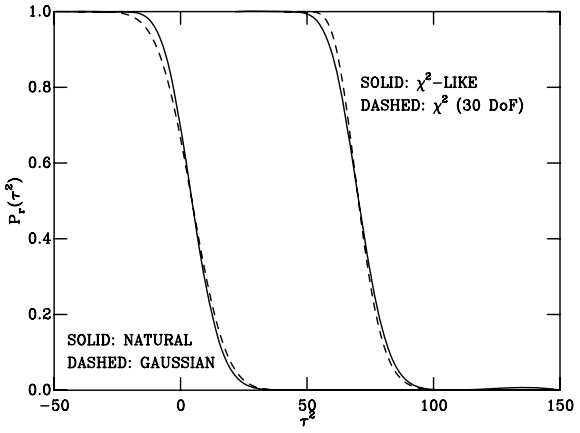


**Figure 3.** The probability of obtaining a given $\tau^2$ for a fit of 30 data points to a MS. This is the distribution one would obtain if one created a large number of data sets at a given distance modulus and extinction, and then 'fitted' the data with the distance modulus and extinction fixed at their original values. The right-hand solid curve is for the $\chi^2$-like normalization, the left-hand solid curve for a natural normalization where the sum of the probability over all colours is independent of magnitude. For comparison, the dashed curves show the $\chi^2$ distribution for 30 degrees of freedom and the Gaussian distribution for $\sigma = 60$, with their expectation values shifted to match those for the $\chi^2$-like and natural distributions, respectively.

## 7 UNCERTAINTIES

We have found a faster method for calculating the uncertainties than that presented in Naylor & Jeffries (2006). The aim of the calculation is to place a contour in the $\tau^2$ grid of Fig. 2 which represents a region within which the parameters lie with a given confidence. We can derive the uncertainties by first converting the values of $\tau^2$ in the grid into probability, and then integrating over the entire grid. We then divide this into the integral of the probabilities below progressively higher values of $\tau^2$ to obtain the cumulative $\tau^2$ distribution. We can then pick off values of $\tau^2$ at given confidence limits, and draw contours on the $\tau^2$ space.

There are four practical issues which have to be solved when using this method. The first is that to carry out the integral one must multiply each pixel by its area. If the axes are linear, then the area of the pixels is the same, and the sum of the pixels will suffice, as we normalize by the integral over the whole area. However, if the age axis is logarithmic, the simplest method is to multiply the probability by the age for that pixel, before performing the sum.

The second problem is the underlying assumption that the model is correct. This means that the fitting to create the grid must be carried out using only those data points which are consistent with the model. So practically this means that a second fit must be carried out excluding any points which the first fit clipped, without any further clipping (see Section 5.4). Even so, this means one fit as opposed to fitting typically 100 Monte Carlo data sets for the previous technique, giving a speed improvement of a factor of 100.

The third issue is that one must sum the grid out to infinity. This is less demanding than it might at first appear. For example, if fitting a single data point in one dimension with Gaussian uncertainties, one only has to move $\pm 3\sigma$ from the best fit to include 99.7 per cent of the total probability, which is accurate enough for calculating a 95 per cent confidence interval. Note, however, that the probability enclosed for a given $\sigma$ declines as the power of the number of observables measured for each data point, and so if generalizing $\tau^2$ to many dimensions one would have to act with caution.

The final issue is that the machine precision may be exhausted for some data points towards the edge of the $\tau^2$ grid, where the corresponding values of $\rho$ are very close to zero. For example, if the smallest representable number greater than zero is $1 \times 10^{-36}$, the highest $\tau^2$ which can be obtained is approximately 168. Once the $\tau^2$ for any data point lies below this probability, the computer will calculate $\tau^2$ for the whole data set to be infinite. To flag such points in the grid, we set them to a high value of $\tau^2$ (the number of data points times the $\tau^2$ resulting from a probability of twice

[1] It is interesting that the differential form of the $\tau^2$ distribution (like the $\chi^2$ distribution) tends towards a Gaussian. This is a natural consequence of the central limit theorem, since multiplying functions together and then taking the logarithm is equivalent to averaging their logarithms. Whilst the mean and width of the distribution are problem-dependent, this may still provide a key to the solution in more general cases.

the smallest representable number). Since such a $\tau^2$ is guaranteed to return a probability of zero, this works transparently in code which implements the new method of calculating confidence limits. However, we also note this number in the header of the grid file, so its meaning is clear if plots are made from the file. Applying this technique to the Cep OB3b data results in the contour shown in Fig. 2.

For the work here, the distance is a nuisance parameter, and we need to be able to quote an uncertainty in age alone. We therefore integrate the probability in Fig. 2 over all distance moduli at each value of the age to create a run of probability with age. We then define a confidence limit as that region in age which integrates to give 68 per cent of the probability, and which excludes equal integrals of probability above and below it. For Cep OB3b, this gives an age range of 8.6–10.9 Myr.

## 8 THE EXTINCTION

Now having shown how we can fit for age, we must return to the question of the extinction. We follow an improved version of the two-strand approach developed in Mayne & Naylor (2008). We first attempt to fit the $U - B/B - V$ data with just the reddening as a free parameter. We can now (in contrast to Mayne & Naylor 2008) test whether the model is a good description of the data. If it is, we assume the extinction is uniform, and apply the derived extinction to all the data points. If $\Pr(\tau^2)$ is too high, we conclude that the extinction is non-uniform and resort to deriving individual extinctions for each star by moving them along the (colour-dependent) reddening vector until they reach the single-star $U - B/B - V$ isochrone. This is essentially a modern version of the $Q$ method of Johnson & Morgan (1953). As explained in Mayne & Naylor (2008), the disadvantage of this method is that it cannot allow for the fact the star may be a binary. This has the effect of narrowing the dereddened sequence in $V/B - V$ space, hence our preference for the $\tau^2$ method where the extinction can be shown to be uniform.

## 9 MAIN-SEQUENCE AGES

We can now apply our technique to the rest of our sample of clusters and associations to derive MS ages. Each data set we fit is given as a (electronic only) table as summarized in Table 1 (see Supporting Information), though we show the data for λ Ori as an example in Table 2.

**Table 1.** MS and PMS ages.

| Cluster or group | PMS age (Myr) | MS age (Myr) Best fit | MS age (Myr) 68 per cent confidence | $\Pr(\tau^2)$ | Distance modulus | $E(B-V)$ | Data table | Numbering system reference |
|---|---|---|---|---|---|---|---|---|
| λ Ori | 3 | 6.6 | 5.8–7.5 | 0.52 | 8.05 | 0.12[1] | 2 | HD catalogue |
| NGC 6530 | 2 | 5.5 | 4.9–6.1 | 0.84 | 10.76 | 0.33[1] | 3 | Walker (1957) |
| NGC 2264 | 3 | 5.5 | 2.4–6.0 | 0.06 | 9.24 | 0.05 | 4 | Walker (1956) |
| ONC | 3 | 5.0 | 2.8–5.2 | 0.10 | 7.92 | 0.03 | 5 | Brun (1935) |
| σ Ori | 3 | 0.4 | < 6.6 | 0.26 | 7.98 | 0.06[2] | 6 | HD catalogue |
| NGC 2362 | 4.5 | 9.1 | 5.4–12 | 0.08 | 10.71 | 0.08 | 7 | Johnson (1950) |
| CepOB3b | 4.5 | 10 | 8.6–10.9 | 0.05 | 8.72 | 0.89[1] | 8 | Blaauw et al. (1959) |
| IC2602 | 25 | 44 | 28–62 | 0.27 | 5.88 | 0.02 | 9 | HD catalogue |
| NGC 2547 | 38 | 48 | 27–62 | 0.13 | 8.03 | 0.04 | 10 | Claria (1982) |
| Pleiades | – | 115 | 104–117 | 0.81 | 5.35 | 0.02[1] | 11 | Hertzsprung (1947) |

[1]Median from individual extinctions.
[2] From Brown et al. (1994).

**Table 2.** A sample of Tables 2–11, the fitted data set for λ Ori. Table 1 gives the number of the electronic table for each data set (see the Supporting Information), along with the reference for the star numbering system. As shown here, for each cluster we give, along with the uncertainties, the fitted $V$, $B-V$ and $U-B$. In the case of groups where extinctions were derived on a star-by-star basis, these are the reddening- and extinction-free values, and the $E(B-V)$ used is given in the last column.

| Star number | $V$ (mag) | $\sigma$ | $B-V$ (mag) | $\sigma$ | $U-B$ (mag) | $\sigma$ | $E(B-V)$ |
|---|---|---|---|---|---|---|---|
| 36822 | 4.036 | 0.010 | −0.270 | 0.008 | −1.047 | 0.010 | 0.120 |
| 36861 | 3.346 | 0.010 | −0.271 | 0.008 | −1.049 | 0.010 | 0.061 |
| 36862 | 4.710 | 0.010 | −0.241 | 0.008 | −0.953 | 0.010 | 0.281 |
| 36894 | 8.662 | 0.010 | −0.086 | 0.008 | −0.295 | 0.010 | 0.036 |
| 36895 | 6.512 | 0.010 | −0.188 | 0.008 | −0.745 | 0.010 | 0.068 |
| 37034 | 8.976 | 0.010 | −0.069 | 0.008 | −0.216 | 0.010 | 0.109 |
| 37035 | 8.249 | 0.010 | −0.141 | 0.008 | −0.562 | 0.010 | 0.121 |
| 37051 | 8.699 | 0.010 | −0.074 | 0.008 | −0.239 | 0.010 | 0.114 |
| 37110 | 8.657 | 0.010 | −0.097 | 0.008 | −0.346 | 0.010 | 0.097 |
| 245140 | 8.568 | 0.010 | −0.107 | 0.008 | −0.398 | 0.010 | 0.217 |
| 245168 | 9.077 | 0.010 | −0.057 | 0.008 | −0.173 | 0.010 | 0.177 |
| 245185 | 9.313 | 0.010 | −0.050 | 0.008 | −0.153 | 0.010 | 0.190 |
| 245203 | 6.972 | 0.010 | −0.188 | 0.008 | −0.745 | 0.010 | 0.158 |

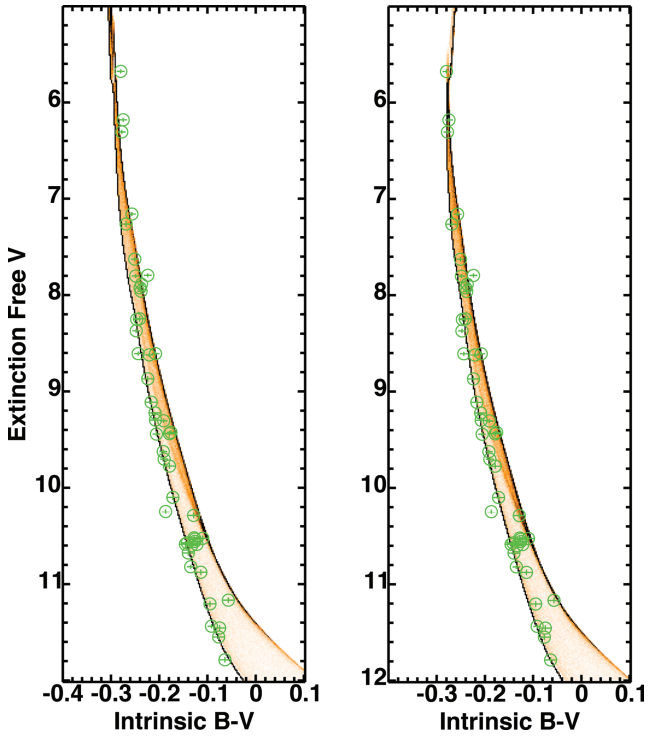


**Figure 4.** The best-fitting model for NGC 6530 with the age fixed at 2 Myr (left-hand panel) and the best-fitting model with both age and distance as free parameters (right-hand panel). Note how the five brightest data points are better fitted in the right-hand panel, and how the group of data points below them would have to be interpreted as binaries in the model in the left-hand panel. The very faintest single stars also lie marginally closer to the single-star sequence in the better-fitting model.

### 9.1 NGC 6530

We used the data and uncertainties of Walker (1957), which are for a sample which is unbiased in colour and taken from a specific area of the cluster. To ensure that we excluded the PMS, we selected only those stars bluewards of $B - V = 0.28$ and brighter than $V = 13$ and derived individual extinctions. The resulting fit is shown in the right-hand side of Fig. 4.

### 9.2 $\sigma$ Ori

Our sample consisted of the members listed by Sherry et al. (2008) that are bluewards of $B - V = 0.1$. We omitted the two stars noted by Sherry et al. (2008) as variable, and HD 37333 which is above the MS, and probably a PMS star. We could not find a consistent Johnson *UBV* data set for this cluster, and so used the Tycho-2 catalogue and its first supplement (Høg et al. 2000b), although it does not contain a magnitude for $\sigma$ Ori C. In this data set, a combined magnitude is given for $\sigma$ Ori A and B. As $\sigma$ Ori A is itself a binary, we removed the effect of $\sigma$ Ori B on the combined magnitude by assuming that the magnitude difference between the components is the mean of the values for the difference found from speckle (Horch, Ninkov & Franz 2001) and adaptive optics (ten Brummelaar et al. 2000) work. $\sigma$ Ori B will have little effect on the combined colour.

The disadvantage of using the Tycho-2 data is that we cannot determine the extinction, as there are no *U*-band data. We therefore simply adopted $E(B - V) = 0.06$ from Brown, de Geus & de Zeeuw (1994). The resulting $\tau^2$ contour does not close at low ages, and so we have only an upper limit on the age. We therefore quote (in Table 1) the upper limit below which 68 per cent of the probability lies, but exclude this cluster from further analysis.

### 9.3 NGC 2264

We used the photoelectric data of Walker (1956), as presented in his table 1. Fitting all stars bluewards of $B - V = 0$ for extinction in $U - B/B - V$ space gives $\Pr(\tau^2)$=0.37, implying uniform extinction over the field. We then fitted in $V/B - V$ and obtained a $\Pr(\tau^2)$ of 0.06. This is on the margins of acceptability, and there is a case that the two data points furthest redwards from the sequence should be removed. However, in not doing so we simply enlarge our uncertainty estimate, and so are being conservative.

### 9.4 λ Ori (Collinder 69)

We used the data from Murdin & Penston (1977) taking only those stars within half a degree of λ Ori. We excluded objects with $B - V > 0.2$, which results in a sample which is almost completely bluewards of this colour and has no stars redwards of $(B - V)_0 = -0.04$. After applying reddenings determined on a star-by-star basis, we obtained a value of $\Pr(\tau^2)$ of 0.52, provided we assumed that the uncertainties were 0.01 mag in $V$ and 0.008 mag in $B - V$ (Murdin & Penston 1977, do not provide error bars) and removed two objects (HD 36881 and HD 36913) which appear to be non-members based on their positions in the $V_0/(B - V)_0$ diagram. The resulting fit is shown in the right-hand side of Fig. 5.

### 9.5 NGC 2362

We used the data and associated uncertainties for NGC 2362 from Johnson & Morgan (1953), which were taken as part of a programme to define what became the *UBV* system. We used only those stars bluewards of $B - V = 0.04$ and excluded stars noted as non-members by Johnson & Morgan (1953). We also excluded the brightest star ($\tau$ CMa) as it is clearly beyond the turn-off. Finally, we found that star 36 gave a high $\tau^2$ in both $U - B/B - V$ and $V/B - V$, and star 50 in $V/B - V$, and so we removed them from the fit as well. We then measured a global extinction from the $U - B/B - V$ diagram, before fitting in $V/B - V$.

### 9.6 Cep OB3b

Blaauw, Hiltner & Johnson (1959) carried out a photometric survey of stars of spectral type A0 and earlier identified from objective prism plates. We take the membership list from Pozzo (2001), but exclude BHJ11 for which the measurement is a combined light measurement for a rather wide $\Delta m = 2.5$ binary. We dereddened this sample on a star-by-star basis. Using the uncertainties quoted in Blaauw et al., we obtain a just about acceptable value of $\Pr(\tau^2) = 0.05$.

### 9.7 The environs of the Orion Nebula Cluster

Our data and uncertainties are taken from Walker (1969), who aimed to obtain photometry for as many stars as possible within the outline of the dark cloud, since this area will be the least contaminated by background stars. We removed stars redwards of $B - V = 0.0$, those marked as variables or visual doubles, and three stars which lie away from the sequence in the $U - B/B - V$ diagram. We fitted the data for a single extinction in $U - B/B - V$ space, and after removing two outliers in $\tau^2$ obtained a good fit with $\Pr(\tau^2) = 0.46$.

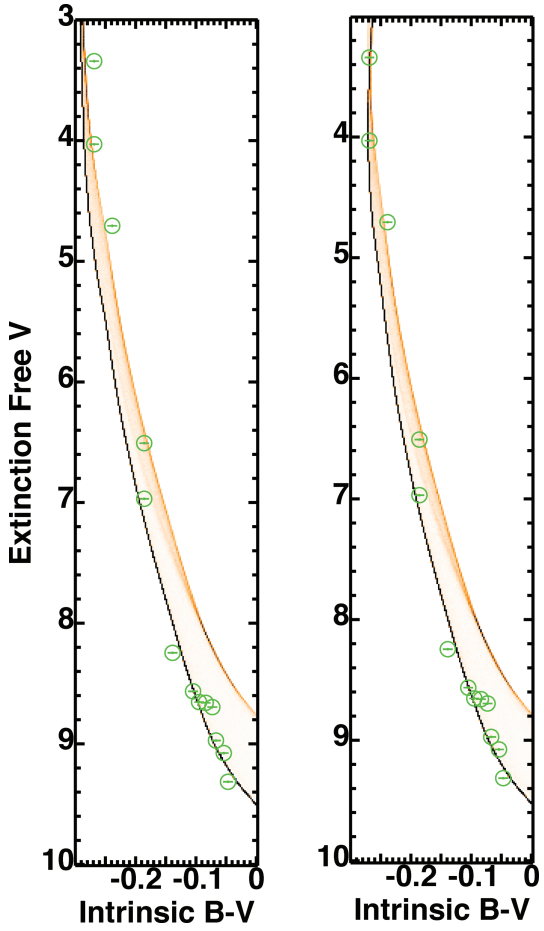


**Figure 5.** The best-fitting model for λ Ori with the age fixed at 3 Myr (left-hand panel) and the best-fitting model with both age and distance as free parameters (right-hand panel). The brightest three stars are clearly better fitted by the model in the right-hand panel.

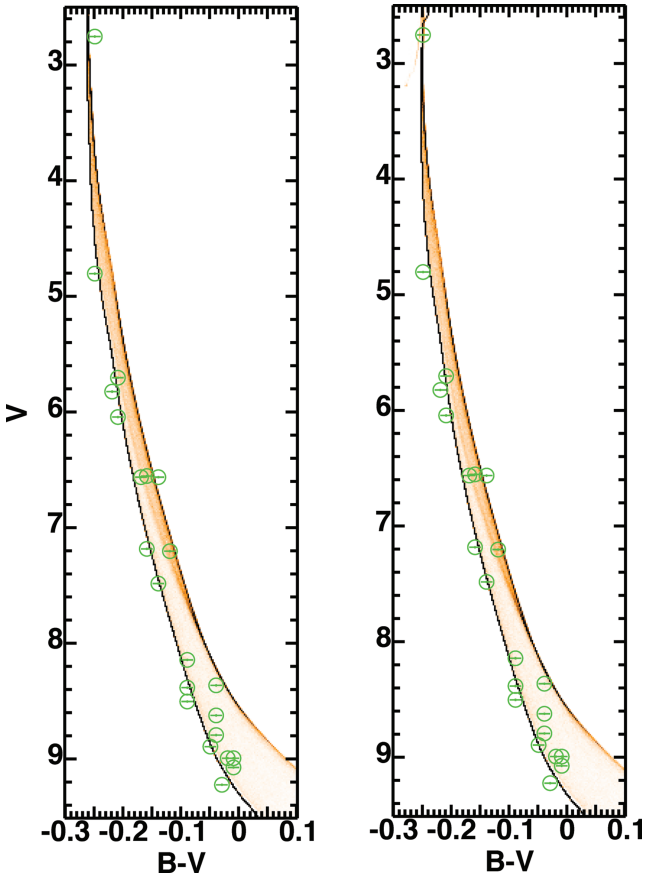


**Figure 6.** The best-fitting model for the ONC with the age fixed at PMS age of 3 Myr (left-hand panel) and the best-fitting model with both age and distance as free parameters (right-hand panel). The 68 per cent confidence interval for the best-fitting age just encompasses 3 Myr, and so we expect the improvement in the fit from left to right to be only marginal. We can see the improvement in the fit is due entirely to the improvement in the fit for the brightest star, and even that is at the expense of a worse fit for the second brightest star. Thus, the conclusion that the statistics drive us to, that the improvement is marginal, seems reasonable.

At first, this may sound counterintuitive, since it implies uniform extinction, yet it is well known that the extinction of ONC members is highly variable. In fact, it seems that this only applies to stars in the central cluster. We then fitted in $V/B-V$ to obtain the results shown in Table 1. The resulting fit is shown in the right-hand side of Fig. 6.

### 9.8 NGC 2547

We took the photometry from Claria (1982), and used an uncertainty of 0.02 mag in both magnitude and colours. This is an estimate for $U-B$ and corresponds to the deviations for single observations derived by Claria (1982) from comparison with the data of Fernie (1959). Although Claria (1982) often has four observations per star, we prefer to take the view that the uncertainty represents the difference between the photometric systems. We use the membership list of Claria (1982), which is based on proper motions, photometry and spectroscopy, and select only stars with $B-V<0.1$ to ensure that we exclude PMS stars. We found that if we included star 40, which appears to sit just below the MS, we obtained an unacceptably low value of $\Pr(\tau^2)$. Furthermore, this star is right on the edge of the proper motion distribution of the bulk of the members, so we excluded it.

### 9.9 IC2602

We used the data of Eggen (1972), excluding stars with $B-V>0.0$, and HD 93163, which lies away from the sequence. Unfortunately, Eggen (1972) does not provide uncertainties, but we found that a single extinction would yield $\Pr(\tau^2)=0.79$ for uncertainties of 0.014 and 0.014 mag in $B-V$ and $U-B$, respectively, which suggests that the extinction is uniform. Using that extinction and an uncertainty in $V$ of 0.025 mag gives $\Pr(\tau^2)=0.27$ when fitted in $V$ versus $B-V$.

### 9.10 The Pleiades

We again used the data and memberships from Johnson & Morgan (1953). The $U-B/B-V$ diagram, especially the region where the gradient is reversed, shows that there is variable extinction to this cluster. We therefore dereddened the data on a star-by-star basis, which limits us to $B-V<0.0$. Before fitting, we also excluded Hertzsprung 371 (which appears to be reddened).

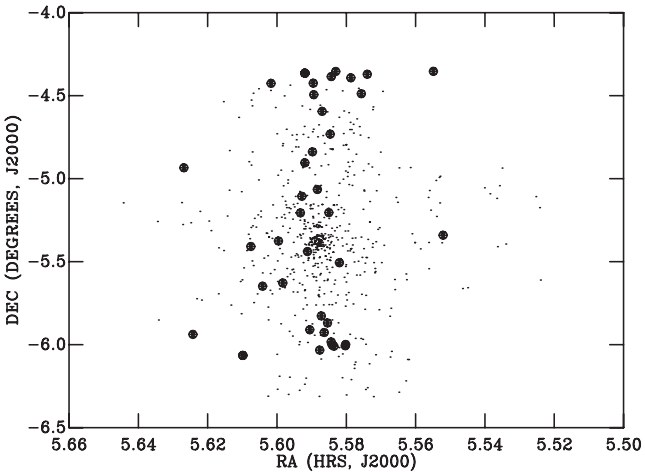


**Figure 7.** The positions of stars in the vicinity of the Orion Nebula Cluster. The dots in the central region are one in five of the stars from Hillenbrand (1997). The dots around the periphery are X-ray sources from Ramírez et al. (2004). The filled circles are the MS sample.

## 10 PRE-MAIN-SEQUENCE AGES

For the PMS ages, we require a set of consistent ages, and therefore adopt the ages of Mayne & Naylor (2008), with the following exceptions.

### 10.1 NGC 2547, IC2602 and Cep OB3b

We take the PMS age for NGC 2547 from Naylor & Jeffries (2006) as 38.5 Myr, which is derived from isochrone fitting, though also agrees with the lithium depletion age. The age for IC2602 (25 Myr) is taken from Stauffer et al. (1997), which again is based on isochrone fitting to the PMS stars. We use a PMS age of 4.5 Myr for Cep OB3b, which is from Littlefair et al. (in preparation), but is based on the system of Mayne & Naylor (2008).

### 10.2 The environs of the Orion Nebula Cluster

The position on the sky of our MS sample is shown in Fig. 7, along with the positions of the sample of Hillenbrand (1997), which represents stars in the ONC itself, and the flanking fields of Ramírez et al. (2004). Given the distribution of stars, it is clear that the PMS age we should use is that of the flanking fields. Although Ramírez et al. (2004) calculate this, they do so on the assumption that the ONC is 470 pc away, whilst a more modern estimate is 400 pc (Mayne & Naylor 2008, and references therein). In the $V_0/(V - I)_0$ diagram, Ramírez et al. (2004) place the flanking fields 0.3 mag above NGC 2264. Correcting the distance to 400 pc will bring the flanking field PMS to the same magnitude as that of NGC 2264, and therefore to an age of 3 Myr on the scale of Mayne & Naylor (2008).

## 11 DISCUSSION

We collect together our measurements of the ages of the groups and clusters in Table 1, along with the other parameters from our fits. For completeness, we include the distances, though as these are derived from two-parameter fits we emphasize that those of Mayne & Naylor (2008) are to be preferred. We plot PMS against MS age in Fig. 8. Whilst the PMS and MS ages for individual clusters may agree to within the uncertainties, the average of the MS ages

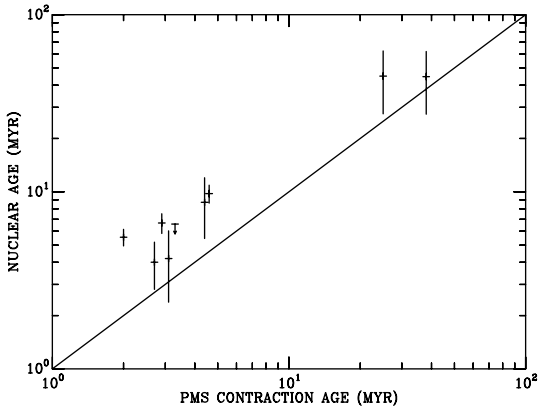


**Figure 8.** The MS and PMS ages for our sample. The groups at PMS ages of 3 and 4.5 Myr have been separated slightly in age to aid visibility.

is significantly older than the average of the PMS ages. If we take only those clusters and associations less than 10 Myr old, the MS ages are, on average, a factor of 2 larger. The issue is clearly which of these age scales is correct.

### 11.1 Are the main-sequence ages incorrect?

Explanations as to why the MS ages may be incorrect fall into two groups, those associated with the statistical techniques and those associated with the models. We can rule out problems with the fitting procedure by comparing our ages with those obtained by Meynet, Mermilliod & Maeder (1993). They use similar isochrones to the ones presented here and measure the age of the Pleiades as 100 Myr and the environs of the ONC as 4 Myr. Both these ages are compatible with those we measure, suggesting our technique gives similar ages to 'by eye' fitting. Equally importantly, our age for NGC 2547 matches its lithium depletion age (34–36 Myr; Jeffries & Oliveira 2005) and our age for the Pleiades is very close to its depletion age (125–130 Myr; Stauffer, Schultz & Kirkpatrick 1998).

To check that our uncertainties are at least reasonable we tested how the result changes if one star is removed from each fit. As one might expect, the brightest star in the fit provides the tightest limits on the age. We therefore removed the brightest star from each data set and replotted Fig. 8. As Fig. 9 shows, the result remains clear, though as one might expect the error bars are larger, and one more data set (the ONC) returns an upper limit for the age.

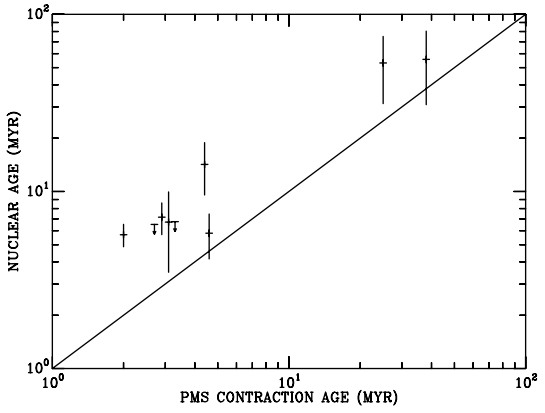


**Figure 9.** As Fig. 8, but with PMS ages calculated without the brightest star for each data set.

This strongly suggests that our uncertainty estimates are reasonable, and the result is robust. This experiment also shows what the effect might be of a non-member being included in the fit. Were a non-member very far from the fitted sequence, it would have been clipped out by the procedure described at the end of Section 5.4. Were it close to the sequence, then it could deviate the fit sufficiently to have a reasonable $\tau^2$, but then would only change the best fit by a small amount, similar to the effect of removing a data point.

As a final check of the uncertainties, in Figs 4–6 we plot the data over the best-fitting models if the age is fixed at the PMS age (left-hand panels) or left as a free parameter (right-hand panels). The first two examples (NGC 6530 and $\lambda$ Ori) are ones where the PMS age lies far outside the 68 per cent confidence region for the upper-MS age. As one expects, we see that the brightest stars lie to the right of the model when the age is fixed at the PMS age. Our final example, the ONC, is one where the PMS age lies almost exactly on the edge of the 68 per cent confidence limit. Here the improvement in the fit is, as it should be, marginal. Although such comparisons with our expectations are at best subjective, that they fit with our expectations adds to our confidence in the result. When combined with the experiment of missing out the brightest data point, we have a strong case that our uncertainties are correct, and the result is robust.

The obvious problems with the models are the absence of rotation, uncertainties as to the mass-loss rates and the treatment of convective core overshoot. Fig. 9 of Meynet & Maeder (2000) shows that if the stars were rotating, and we fitted them with isochrones for stationary stars, the resulting ages would be too young by about 10 per cent. This therefore exacerbates the discrepancy between the PMS and MS ages.

All modern models include a degree of core overshoot, which has the effect of mixing more hydrogen into the core, and hence lengthening the MS lifetime. Naively, models with no overshoot will have shorter MS lifetimes than those used here, by roughly the decrease in available hydrogen (perhaps 20–40 per cent), which is of the right order to bring the MS and PMS ages back into agreement. However, our CMD fitting does not measure lifetime on the MS, but how far from the ZAMS a star at a given luminosity (not mass) has moved. A close comparison of figs 4 and 5 of Maeder & Mermilliod (1981) shows that for the youngest ages they calculate (25 Myr) the difference in the position of the isochrone corresponds to an age difference of around 5 per cent.

Mass-loss rates for early-type stars are uncertain, and so in addition to using the Geneva models with the standard mass-loss rates (set 'c' of Maeder & Meynet 1994) we also tried the higher mass-loss rate, set 'e'. Comparison of the resulting isochrones for the masses and ages we are interested in shows differences in colour which are too small to affect our results.

Finally, we have tested the effect of using different MS models. As an alternative to the Geneva models with the Bessell et al. (1998) conversions to colour and magnitude we used the conversions presented with the isochrones in Lejeune & Schaerer (2001). We obtained ages somewhat older than those from the Geneva–Bessell models, exacerbating the age difference problem. More importantly, the values of $\Pr(\tau^2)$ are much worse than those for the Geneva–Bessell models, typically around 0.01 or 0.001, showing that these models can be ruled out as good descriptions of the data. To test whether this is the interior models or the atmospheres, we fitted the data to the Padova models (Girardi et al. 2002) but with the same model atmospheres (Bessell et al. 1998) as we used for the Geneva–Bessell models. We find that this gives slightly younger ages (a factor of 1.5 older than the PMS ages in the range 1–10 Myr), but very similar values of $\Pr(\tau^2)$ to the Geneva–Bessell models. In summary, therefore, our fitting gives strong support to the Bessell et al. (1998) conversions, and there is only a weak effect from the interior models, which can explain some, but not all of, the age discrepancy.

### 11.2 Are the pre-main-sequence ages incorrect?

The PMS ages are much less robust than the MS ones. We have adopted the PMS age scale of Mayne & Naylor (2008). However, as Mayne & Naylor (2008) and Mayne et al. (2007) make clear, the primary aim of this scale is an age ordering. The age scale itself is rather arbitrary, though was chosen to match as closely as possible the commonly quoted ages for the young groups. The problem is that there is no single PMS age scale, a point nicely illustrated in Jeffries et al. (2009). They show that the $\gamma$ Vel association could have a PMS age between 5 and 15 Myr depending on which PMS models are used, and which part of the sequence is considered. They estimate that the association is about 7 Myr old on the Mayne & Naylor (2008) scale, so doubling the ages of these young associations is consistent with some PMS models. Our conclusion, therefore, is that the MS age scale is probably the correct one.

### 11.3 Implications of lengthening the PMS time-scale

Before discussing the implications of a longer time-scale, we should be wary of overinterpreting Fig. 8. Whilst it clearly shows a discrepancy between mean PMS and MS ages, the error bars for individual data points are large. All we can say with any certainty is that there is a difference of approximately a factor of 2 at PMS ages of 3 Myr. By 30 Myr, our data are consistent with the age scales matching, though a difference of a factor of 1.5 is still, in the statistical sense, likely. We therefore limit ourselves to discussing the implications of a lengthening of the time-scales in the 1–10 Myr PMS age range. Even here, however, we find that there are problems it might solve.

There is a long-standing issue that the observed time-scale for the dissipation of protostellar discs (3 Myr; Haisch, Lada & Lada 2001) may be shorter than the time required by the models for planet formation (10 Myr; Pollack et al. 1996). In recent years, there has been significant effort to find mechanisms which will shorten the planet-forming time-scales. Whilst a case can be made that this problem has been solved (Mordasini et al. 2008), there is a view that significant problems remain (see e.g. the introductory sections of Dodson-Robinson et al. 2008; Ayliffe & Bate 2009). A fair summary is probably that whilst there are mechanisms which could shorten the time-scale, such as dust settling (Hubickyj, Bodenheimer & Lissauer 2005) and planetary migration (Alibert et al. 2005), the uncertainties in the physics remain such that it is not clear if they do. Our result offers an interesting alternative solution. If the clusters used to measure the disc dissipation time-scale are 50–100 per cent older than previously thought, there may be no contradiction with the Pollack et al. (1996) time-scale.

Jeffries et al. (2007) point out that there is a lack of clusters in the age range 5–30 Myr. Revising the age scale in the way suggested by the MS fitting would move clusters from the youngest ages into this age range. Furthermore, if the age scales come back into register at around 30 Myr, as Fig. 8 suggests they might, there would not be a compensating movement out of the 5–30 Myr range, leading to an increased number of clusters at these ages.

## 12 CONCLUSIONS

We have shown that there is a systematic difference between the ages of clusters and associations measured from the MS and ages commonly used which are based on the PMS. The difference is in the sense that the MS ages are a factor of 1.5–2.0 greater than the PMS ages in the age range 2–5 Myr (on the PMS scale). The most straightforward solution is to adopt the MS age scale, as there are PMS models which fit with the longer time-scale. Adopting the longer time-scale offers a solution to the problem that the lifetimes of discs around stars (3–5 Myr on the PMS age scale) are shorter than the time taken to form planets, and to the apparent absence of clusters in the 5–30 Myr age range.

Finally, we should be clear that although we favour the age-scale given by MS fitting, we are not recommending it as a method for deriving ages for individual clusters and associations. As Fig. 8 and Table 1 make it clear, the uncertainties for individual groups are large. Nor can we at this point make any clear recommendation as how one should reflect this result when quoting PMS ages. Whilst it is clear that the youngest ages need to be increased, how far down the age scale that should be propagated is unclear. We therefore continue to commend the Mayne et al./Mayne & Naylor age ordering, though recommend that if these ages are quoted one clearly states that they are on the Mayne et al./Mayne & Naylor scale. If absolute ages are required for clusters younger than 10 Myr for comparison with other data, we recommend multiplying the Mayne et al./Mayne & Naylor values by 1.5 and quoting the age scale as originating from this paper.

## ACKNOWLEDGMENTS

I am grateful to three people for provoking significant parts of this work. First, Herbie (H.D.) Deas for conversations many years ago demonstrating that one has choices in mathematics; a view which led me to the re-examination of the normalization presented in Section 5.2. Secondly, the (anonymous) referee of Naylor & Jeffries (2006), whose efforts emphasized to me the inelegance of the method presented in that paper for calculating the uncertainties in the parameters, and hence led to Section 7. Thirdly, the referee of a very early version of this paper forcefully made the point that it would be improved by the inclusion of data, which led me to the main result presented here.

This research has made use of the WEBDA data base, operated at the Institute for Astronomy of the University of Vienna, from where much of the electronic form of the data used here originated. Finally, the referee of this version of the paper, John Stauffer, prompted several improvements.

## REFERENCES

Alibert Y., Mousis O., Mordasini C., Benz W., 2005, ApJ, 626, L57
Ayliffe B. A., Bate M. R., 2009, MNRAS, 393, 49
Bessell M. S., 2000, PASP, 112, 961
Bessell M. S., Castelli F., Plez B., 1998, A&A, 333, 231
Blaauw A., Hiltner W. A., Johnson H. L., 1959, ApJ, 130, 69
Brown A. G. A., de Geus E. J., de Zeeuw P. T., 1994, A&A, 289, 101
Brun A., 1935, Publ. Obs. de Lyon, 1, 12
Claria J. J., 1982, A&AS, 47, 323
Dodson-Robinson S. E., Bodenheimer P., Laughlin G., Willacy K., Turner N. J., Beichman C. A., 2008, ApJ, 688, L99
Eggen O. J., 1972, ApJ, 173, 63
Fernie J. D., 1959, Mon. Notes Astron. Soc. South. Afr., 18, 57
Girardi L., Bertelli G., Bressan A., Chiosi C., Groenewegen M. A. T., Marigo P., Salasnich B., Weiss A., 2002, A&A, 391, 195
Haisch K. E., Jr, Lada E. A., Lada C. J., 2001, ApJ, 553, L153
Hertzsprung E., 1947, Anlei, 19, 1
Hillenbrand L. A., 1997, AJ, 113, 1733
Høg E. et al., 2000a, A&A, 357, 367
Høg E. et al., 2000b, A&A, 355, L27
Horch E., Ninkov Z., Franz O. G., 2001, AJ, 121, 1583
Hubickyj O., Bodenheimer P., Lissauer J. J., 2005, Icarus, 179, 415
Jeffries R. D., Oliveira J. M., 2005, MNRAS, 358, 13
Jeffries R. D., Oliveira J. M., Naylor T., Mayne N. J., Littlefair S. P., 2007, MNRAS, 376, 580
Jeffries R. D., Naylor T., Walter F. M., Pozzo M. P., Devey C. R., 2009, MNRAS, 393, 538
Johnson H. L., 1950, ApJ, 112, 240
Johnson H. L., Morgan W. W., 1953, ApJ, 117, 313
Joshi H., Kumar B., Singh K. P., Sagar R., Sharma S., Pandey J. C., 2008, MNRAS, 391, 1279
Lejeune T., Schaerer D., 2001, A&A, 366, 538
Maeder A., Mermilliod J. C., 1981, A&A, 93, 136
Maeder A., Meynet G., 1994, A&A, 287, 803
Mayne N. J., Naylor T., 2008, MNRAS, 386, 261
Mayne N. J., Naylor T., Littlefair S. P., Saunders E. S., Jeffries R. D., 2007, MNRAS, 375, 1220
Meynet G., Maeder A., 2000, A&A, 361, 101
Meynet G., Mermilliod J.-C., Maeder A., 1993, A&AS, 98, 477
Mordasini C., Alibert Y., Benz W., Naef D., 2008, in Fischer D., Rasio F. A., Thorsett S. E., Wolszczan A., eds, ASP Conf. Ser. Vol. 398, Giant Planet Formation by Core Accretion. Astron. Soc. Pac., San Francisco, p. 235
Murdin P., Penston M. V., 1977, MNRAS, 181, 657
Naylor T., Jeffries R. D., 2006, MNRAS, 373, 1251
Pollack J. B., Hubickyj O., Bodenheimer P., Lissauer J. J., Podolak M., Greenzweig Y., 1996, Icarus, 124, 62
Pozzo M., 2001, PhD thesis, Univ. Keele
Ramírez S. V. et al., 2004, AJ, 128, 787
Schaller G., Schaerer D., Meynet G., Maeder A., 1992, A&AS, 96, 269
Sherry W. H., Walter F. M., Wolk S. J., Adams N. R., 2008, AJ, 135, 1616
Stauffer J. R., Hartmann L. W., Prosser C. F., Randich S., Balachandran S., Patten B. M., Simon T., Giampapa M., 1997, ApJ, 479, 776
Stauffer J. R., Schultz G., Kirkpatrick J. D., 1998, ApJ, 499, L199
ten Brummelaar T., Mason B. D., McAlister H. A., Roberts L. C., Jr, Turner N. H., Hartkopf W. I., Bagnuolo W. G. Jr., 2000, AJ, 119, 2403
Walker M. F., 1956, ApJS, 2, 365
Walker M. F., 1957, ApJ, 125, 636
Walker M. F., 1969, ApJ, 155, 447

## SUPPORTING INFORMATION

Additional Supporting Information may be found in the online version of this article.

**Tables 2–11.** The fitted data sets.

Please note: Wiley-Blackwell are not responsible for the content or functionality of any supporting information supplied by the authors. Any queries (other than missing material) should be directed to the corresponding author for the article.

This paper has been typeset from a TEX/LATEX file prepared by the author.